Biosensors and Bioelectronics 106 (2018) 117–121

Contents lists available at ScienceDirect

Biosensors and Bioelectronics

journal homepage: www.elsevier.com/locate/bios

# TriPleX™ waveguide-based fluorescence biosensor for multichannel environmental contaminants detection

Lanhua Liu[a,1], Didi Shan[a,1], Xiaohong Zhou[a,*], Hanchang Shi[a], Baodong Song[a], Floris Falke[b], Arne Leinse[b], René Heideman[b]

[a] State Key Joint Laboratory of ESPC, Research Centre of Environmental and Health Sensing Technology, School of Environment, Tsinghua University, China
[b] LioniX International BV, Netherlands

ARTICLE INFO

*Keywords:*
Biosensor
TriPleX™ waveguide
Evanescent wave
Fluorescence
Environmental contaminants

ABSTRACT

In order to realize the multi-analyte assays for environmental contaminants, an optical biosensor utilizing laser-induced fluorescence-based detection via the binding of biomolecules to the surface of an integrated TriPleX™ waveguide chip on a glass substrate (fused silica, FS) is described. As far as we know, this is the first demonstration of using the TriPleX™ technology to fabricate the waveguide chip on a FS substrate. The sensor consists of 32 individually addressable sensor patches, which were formed on the chip surface by exploiting 3 Y-junction splitters, creating four equal rows of eight evanescently excited windows in parallel. The basic low-loss $SiO_2$/$Si_3N_4$ TriPleX™ waveguide configuration in combination with on-chip spotsize convertors allows for both high fiber-to-chip coupling efficiency and enables at the same time individually optimized high chip surface intensity and low patch-to-patch deviation. Moreover, the complementary metal-oxide-semiconductor compatible fabrication of waveguide chip allows for its mass production at low cost. By taking MC-LR, 2,4-D, atrazine and BPA as the model analytes, the as-proposed waveguide based biosensor was proven sensitive with the detection limits of 0.22 μg/L for MC-LR, 1.18 μg/L for 2, 4-D, 0.2 μg/L for atrazine and 0.06 μg/L for BPA. Recoveries of the biosensor towards simultaneous detection of MC-LR, 2, 4-D, atrazine and BPA in spiked real water samples varied from 84% to 120%, indicating the satisfactory accuracy of the established technology.

## 1. Introduction

The need for sensitive chemical and biochemical sensors capable of multi-analyte detection in a single sample in the fields of environment, medical care, food, anti-terrorism etc. has become extremely important over the past few decades (Heideman et al., 2012; Lambeck, 1992, 2006; Zhu et al., 2013). Natural toxins, agricultural chemical agents (such as pesticides), industrial chemical agents (such as endocrine disrupting substances) etc. are serious threats for public health (Damen et al., 2014; Shi et al., 2013). The conventional chemical analysis methods for contaminant detection are sensitive and reliable; however, they need complicated and time-consuming pre-concentration procedures, expensive testing cost, and rely on large-scale analytical instruments, which would hinder their applications in some cases, such as in-field and on-line testing (Singh et al., 2012). Therefore many researches focus on multi-analyte sensor development and address the problems inherent in discriminating multiple simultaneous signals without loss in measurement speed, specificity or sensitivity (Ligler et al., 1998).

Integrated optical sensors have proven to be a reliable optical platform for fulfilling these requirements, which combine high sensitivity, miniaturization and possibility of mass-production (Heideman et al., 2012). Most integrated optical sensors are constructed based on the evanescent field detection principle, which show a lot of advantages, such as low background and high sensitivity and selectivity (Colomer-Farrarons et al., 2011; Robbins et al., 2004), acting as a beneficial supplement to traditional chemical analysis techniques. Although various types of integrated optical sensors have been reported in the past (Liu et al., 2017c; Robbins et al., 2004; Wiki et al., 2001), the TriPleX™ waveguide-based optical device receives a lot of attentions because of its remarkable advantages, such as ultra-low optical loss and high configuration flexibility (Duer et al., 2010; Leinse et al., 2012; Prak et al., 2011; Wörhoff et al., 2015). In addition , the TriPleX™ waveguide comprises of alternating CMOS compatible low pressure chemical vapor deposition (LPCVD) layers, which are completely transparent for wavelengths from UV to IR (Heideman et al., 2007). This technology also allows for production of low, moderate and high

* Corresponding author.
*E-mail address:* xhzhou@mail.tsinghua.edu.cn (X. Zhou).
[1] Equally contributed to this work.

https://doi.org/10.1016/j.bios.2018.01.066
Received 30 December 2017; Received in revised form 26 January 2018; Accepted 30 January 2018
Available online 01 February 2018
0956-5663/ 

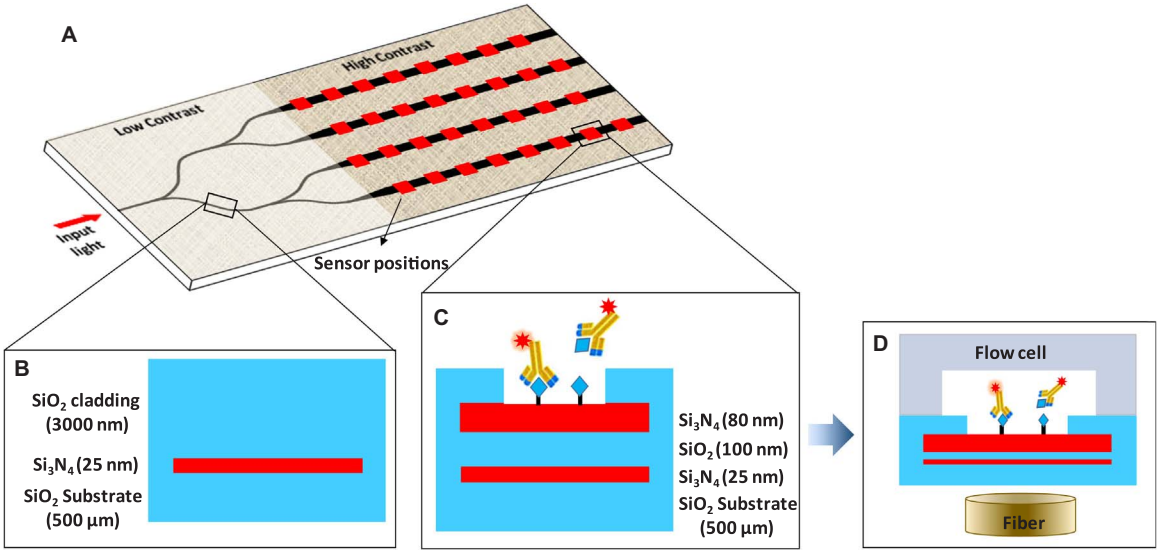


**Fig. 1.** (A) Schematic diagram of the waveguide chip layout; (B) Cross-section of the optimized single-stripe waveguide structure; (C) Cross-section of the optimized double-stripe waveguide structure and the sensing windows for surface chemistry (D) with the integration of flow cell and polymer fiber for fluorescence collection.

refractive index contrast waveguide geometries (Fédéli et al., 2013). Moreover, the standardized silicon microelectronic technologies guarantee the waveguide devices with the great material homogeneity and the possibility of integrating a complete micro optical system with flexible functions on a single chip. Consequently, different types of TriPleX™ waveguide-based optical sensor have been reported and investigated. Most of them are label free to result in the refractive index sensing, such as microring resonators (MRRs) sensors (Besselink et al., 2016; De Vos et al., 2007; Xu et al., 2008) and Mach-Zehnder interferometer (MZI) sensors (Chalyan et al., 2016; Densmore et al., 2006; Misiakos et al., 2014); however, compared with the fluorescent labeling system, most of such biosensors suffer from limited sensitivity. Even so, to our best knowledge, researches on design of the TriPleX™ waveguide for fluorescent biosensing are still rare.

To meet the technological gap, we developed a 32-analyte integrated optical fluorescence biosensor (IOFB) by designing the TriPleX™ waveguides on a glass (e.g. FS) substrate, to allow for simultaneous detection from the bottom side, and fluid manipulation from the top as shown in Fig. 1. The standard silicon microelectronic technology was exploited for the realization of a multi-channel photonic pattern integrated on one chip, distributing the evanescent excitation light into four-channel branches through the Y-junction splitter. By introducing the indirect competition immunoassay, the waveguide surface was modified with antigen-protein conjugate. Four chemical compounds of great environmental significance, including microcystin-LR (MC-LR), 2, 4-dichlorophenoxyacetic acid (2, 4-D), atrazine and bisphenol-A (BPA), were chosen as a paradigm to validate this system capable of multi-contaminant detection in a single water sample. As far as we know, this is the first demonstration that using the TriPleX™ waveguide technology to fabricate the fluorescent integrated chip on a fused silica substrate for environmental bioassay.

## 2. Experiment

### 2.1. Materials

All chemicals and buffers used in this work can be found in Supplementary Information, **Page 2**.

### 2.2. Waveguide geometry design, fabrication and instrumentation

Considering that most evanescent wave fluorescence biosensors used 520 nm or 635 nm diode laser as the excitation light (Anderson et al., 1996; Han et al., 2016; Huang and Tseng, 2005; Liu et al., 2017a, b), an integrated multi-channel waveguide chip was built using the TriPleX™ technology on a glass (eg FS) substrate, providing the evanescent field with high surface intensity, low loss, good patch-to-patch uniformity both at the wavelength of 520 nm and 635 nm, respectively. The TriPleX™ technology is based on LPCVD processes in which silicon nitride ($Si_3N_4$) and silicon oxide ($SiO_2$) are the key materials. These materials have an opposite stress when deposited on a silicon wafer (nitride is tensile and oxide is compressive), therefore stacking them in a multilayer results in a macroscopically low stress layer stack. A variety of geometries can be realized by using LPCVD fabrication process, depending on the different etch depth, layer thickness and waveguide width. Three “standard” TriPleX™ geometries, named as box shape, double–stripe and single–stripe, are extensively studied (Fédéli et al., 2013). Herein, a multilayer-stack of $Si_3N_4$ and $SiO_2$ based waveguide chip with 65 mm × 20 mm in the area and 1 mm in depth was proposed to distribute the laser light into 4 branches with 32 separate sensing windows, as shown in Fig. 1**A**.

Figs. 1**B and** 1**C** show the cross-sectional view of two TriPleX™ geometries connected on the chip and windows exposed for the surface chemistry. In the waveguide design, the single–stripe geometry was adopted in the low refractive index contrast area to achieve an optimal coupling efficiency of light from the single-mode fiber to waveguide and to maintain a single-mode transmission area needed for an even split ratio of the power into different waveguide branches. The double–stripe geometry was adopted in the high refractive index contrast area to achieve an optimal intensity of the evanescent field on the surface for better fluorescent excitation. The transition from low contrast (single stripe) to high contrast (double stripe) area was based on an adiabatic change of waveguide thickness from the single waveguide to the double stack waveguide (see Fig. S1). The resulting on-chip spotsize convertors were very low loss, and allowed for individual optimization of the both fiber-to chip coupling section and the sensing windows. Meanwhile, the waveguide width was altered from 1 to 30 µm, using an adiabatic increase in width of the waveguide. The $Si_3N_4$ layer in the high contract area was exposed to form the sensing window with area of 0.8 mm × 1.5 mm. An extensive simulation was carried out in order to optimize the waveguide chip design (see Section 3.1). The fabrication process was conducted by using the CMOS compatible TriPleX™ waveguide fabrication scheme as depicted in Fig. S1 (Supplementary Information, **Page 3–4).**

The experimental configuration of integrated optical fluorescent biosensor (IOFB) based on the TriPleX™ waveguide is shown in Fig. S2. More description can be found in Supplementary Information, **Page 5**.

### 2.3. Covalent attachment of the hapten-protein conjugates to biosensor chips

To assure reusability of chemically modified chip surface without compromising the binding properties of the immobilized biomolecules, the hapten-protein conjugates (MC-LR-BSA, 2, 4-D-BSA, atrazine-BSA and BPA-BSA) were covalently attached on the chip surface at four randomly selected biosensing spots in four different channels (Fig. S3). A surface modification procedure was used according to our previously reported methods (Liu et al., 2017a; Long et al., 2008), as shown in Fig. S4. More information can be found in Supplementary Information, **Page 9**.

### 2.4. Multi-analyte detection procedure

An indirect competitive immunoassay approach was adopted to analyze the test samples with multiple analytes. The solution containing the mixed and predefined concentrations of Cy5.5-labeled antibodies were pre-incubated with the test sample for 5 min and then injected into the waveguide channels for another incubation of 10 min. The higher concentration of analyte would cause more antibody binding sites occupied, therefore, less Cy5.5-labeled antibodies were captured on the waveguide surface. Consequently, the fluorescent intensity was inversely related to the concentration of analyte in test samples. After that, the waveguide chip surface was washed with SDS (0.5%, pH 1.9) at a flow rate of 1 mL/min for 5 min to remove the antibodies bound to the chip surface, then followed with 3 min wash with PBS at a flow rate of 1 mL/min, ready for a new test cycle. The entire test cycle time was no more than 25 min.

## 3. Results and discussion

### 3.1. Simulation and design of integrated optical waveguide chip

To achieve the maximum fiber-to-chip coupling efficiency and the minimum bend loss at both wavelengths, while maintaining the single-mode transmission behavior for the lowest (520 nm) wavelength, the single–stripe waveguide dimensions were optimized, as shown in Figs. S5 and S6. Under the optimum single–stripe waveguide dimension with a thickness of 25 nm and a width of 1 μm, the fiber to chip coupling efficiencies were −6.5 dB for TE mode at 520 nm, −3.1 dB for TE mode at 635 nm, −1.6 dB for TM mode 520 nm and −0.4 dB for TM mode at 635 nm. The bend radius in the splitter area should be greater than 1.5 mm when only considering TE mode at both wavelengths, but greater than 60 mm when only considering TM mode at both wavelengths.

To achieve the maximum excitation efficiency at both wavelengths in the double–stripe waveguide area, the thickness of the top nitride layer was simulated by assuming that the distance of the fluorophore to the top nitride interface was 10 nm. Fig. 2 shows the simulated variations of excitation efficiency of waveguide with the thickness of the upper stripe in the range of 50 nm and 200 nm. The optimum top nitride thickness was 75 nm for TE mode at 520 nm, 85 nm for TE mode at 635 nm, 105 nm for TM mode at 520 nm and 125 nm for TM at 635 nm.

To avoid the interaction of the evanescent field with outer environment besides the detection area, the top cladding is required to keep the evanescent field inside the sensor chip. The evanescent field will have the longest tail in the area where the effective refractive index of the waveguide will be minimal (Axelrod et al., 1984; Hirschfeld, 1965). Simulation of the minimal required top cladding thickness in the TriPlex™ single-stripe waveguide area for both wavelengths and polarizations is shown in Fig. S7. The thickness of the cladding in the low reflective index contrast area is greater than 2500 nm was suitable for TE mode at both wavelengths, but greater than 8000 nm for TM mode at both wavelengths.

Table S1 illustrates the summary of the above-mentioned simulation results (Supplementary Information, **Page 17**). It was concluded that the TM mode was not beneficial for an optimal excitation point of view regarding the fact that a minimal bend radius of 60 mm, a top cladding of 8 μm and a nitride layer thicker than 100 nm were impractical in chip size and fabrication. Hence, only TE polarized light was considered in the following discussion of design parameters. To compromise the waveguide performance at both wavelengths of 635 nm and 520 nm, the bend radius in the splitter area was set to 2.5 mm, which was well above the simulated minimum of 1.5 mm at 635 nm. With the high contrast area, the thickness of the top nitride layer was set to 80 nm which was the average between both optimal peak values of the chosen wavelengths. The thickness of the cladding layer was set to 3000 nm to maintain the evanescent field inside the sensor chip.

Based on this design, the devices were fabricated by LioniX International. The resulting devices were tested extensively: the obtained experimental results on the individual optical components are in good agreement with the designs. A microscope image of the waveguide splitter structure and etched sensing window is shown in Figs. S8 **A and B**. The excitation light was coupled into the waveguide to form four waveguides for multi-channel biosensing. Photograph image taken from the tested chip using 635 nm red light is shown in Fig. S9. The gray scale intensity plot shown in the inset is the scanning line at the yellow line marks. It shows that in the low contrast area, the excitation light is equally split into four waveguide branches through the Y-junction splitter.

### 3.2. Immunoassay

Firstly, the IOFB system was validated with the response signals on the thirty-two sensing spots towards the same concentration of $10^{-7}$ mol/L Cy5.5 dye solution and the Cy5.5 dye solutions at series concentrations. The relative standard deviation of peak values for the different spots was 24%. The similar result regarding the spot-to-spot nonuniformity were reported in other array optical biosensors (Hua et al., 2005; Liu et al., 2017a). The calibration curves of Cy5.5 dye on two spots with the biggest difference in the response signals is shown in Fig. S10. The detection limit towards the Cy5.5 dye reached 1 nM, which was comparable with other reported array optical biosensors (Hua et al., 2005; Liu et al., 2017a). Results also indicated that the IOFB was sensitive enough to be used for the surface-based immunoassay.

Because the indirect competitive immunoassay was adopted in the IOFB system, the concentration of labeled antibody was proven to be an important factor and strongly affect the sensitivity of detection (Hua et al., 2005; Liu et al., 2017c; Mauriz et al., 2006). To improve the sensitivity of the IOFB system, the effect of Cy5.5-labeled antibody concentration on the signals of IOFB were investigated and illustrated in Fig. S11. Through curve-fitting with the four-parameter logistic function (Supplementary Information, **Page 18**), the linear ranges between the Cy5.5-labeled antibody concentrations and the fluorescence signals were calculated to be 0.9 μg/mL to 1.4 μg/mL for anti-MC-LR antibody, 0.5 μg/mL to 2.4 μg/mL for anti-2,4-D antibody, 0.6 μg/mL to 1.8 μg/mL for anti-atrazine antibody and 0.6 μg/mL to 1.9 μg/mL for anti-BPA antibody. To compromise the reagent costs and the detection sensitivity, the labeled antibody concentrations were selected to be 0.9 μg/mL for anti-MC-LR antibody, 0.5 μg/mL for anti-2,4-D antibody, 0.6 μg/mL for anti-atrazine antibody, and 0.6 μg/mL for anti-BPA antibody.

### 3.3. Simultaneous detection of analytes by using IOFB

Fig. 3 shows the typical calibration curves of using the IOFB system for detection of MC-LR, 2, 4-D, atrazine and BPA in series

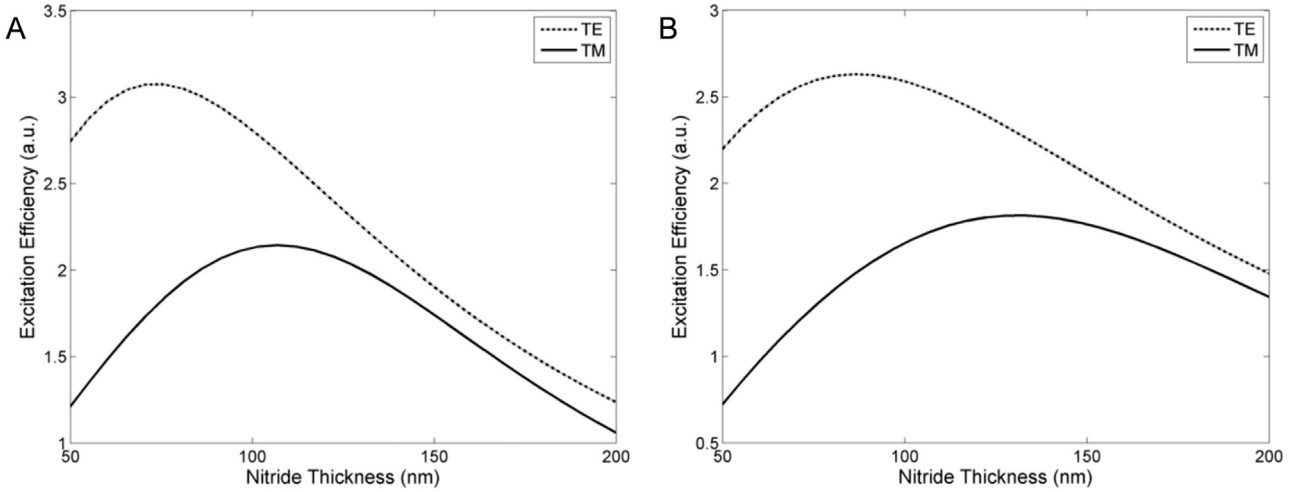


**Fig. 2.** Intensity at the surface of the waveguide as a function of the thickness of the upper stripe. The excitation wavelength is (A) 520 nm and (B) 635 nm, respectively.

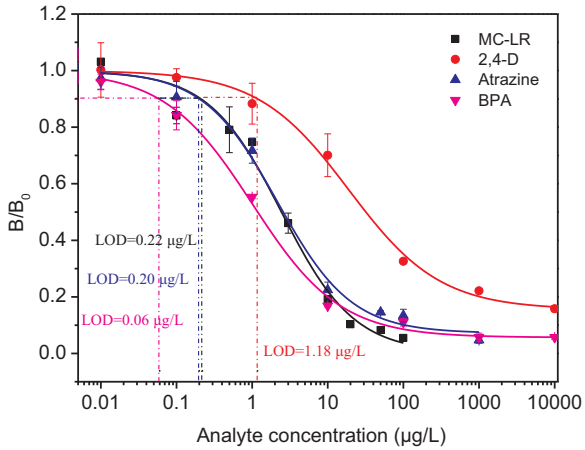


**Fig. 3.** Logistic-fitted calibration curves for the determination of MC-LR, 2,4-D, atrazine and BPA by using the IOFB system.

concentrations in one test sample. As the concentration of analyte in the sample increases, more Cy5.5-labeled antibody is bound to free analyte and therefore prevented from binding to the sensor surface, with the result that the fluorescent signal is lowest for the highest concentrations of analyte (Liu et al., 2017a). With four-parameter logistic fit (Supplementary Information, **Page 18**), the detection limits were calculated to be 0.22 μg/L for MC-LR, 1.18 μg/L for 2, 4-D, 0.2 μg/L for atrazine and 0.06 μg/L for BPA. All of them met the requirements for determining these contaminants in Chinese Surface Water Standard (GB3838-2002). The linear responses ranged from 0.53 μg/L to 11.28 μg/L for MC-LR, 2.79 μg/L to 130.16 μg/L for 2,4-D, 0.45 μg/L to 10.30 μg/L for atrazine, and 0.16 μg/L to 6.43 μg/L for BPA. Results confirmed the application feasibility of using IOFB for achieving the simultaneous detection of multiplex contaminants in one sample. It was also very attractive that one complete test cycle could be obtained less than 20 min. More importantly, performance of the established IOFB system was comparable with other previously reported optical biosensors (Lin et al., 2016; Liu et al., 2017c; Long et al., 2009, 2014; Zhou et al., 2014b), validating the practicability of this system for simultaneous detection of contaminants in water samples.

### *3.4. Regeneration and recoveries*

Compared with the disposable sensing probes, reusable biosensors need fewer preparation steps and shorter operating time. Large quantities of samples could be continuously detected, which paves the way toward automated on-line monitoring of environmental contaminants (Homola, 2003; Shi et al., 2013). To achieve the goal, the hapten-BSA conjugates were covalently immobilized on the chip surface to enhance the stability and reusability of the waveguide. The 0.5% SDS solution (pH 1.9) was used as the regeneration agent and pumped into the flow cell at a flow rate of 1 mL/min. Similar as our previous studies (Liu et al., 2014, 2017a; Zhou et al., 2014a, b), the IOFB waveguide chip surface was robust and could tolerate hundreds of measurement cycles. The relative standard deviation was less than 5% for twenty successive measurements by using the same transducer towards the same test sample.

In order to investigate the practicability of the proposed method, a recovery study was performed, in triplicate, using three real water samples (tap water, lake water taken from the Tsinghua campus and bottled water from the local supermarket, respectively) with two different spiked concentrations. Moreover, the fluorescence signals were checked to be the same as those responding to the buffer solution before the water samples were spiked with the analytes. The concentrations measured were compared with the concentrations spiked and results are summarized in Table S2 (Supplementary Information, **Page 19**). The average recoveries using IOFB system varied from 84% to 120%. Satisfactory variations were also demonstrated with a relative standard deviation of less than 15%. Results indicated the satisfactory accuracy of the established biosensor and confirmed the application potential of this proposed method to measure contaminants simultaneously in real water samples.

## 4. Conclusions

In summary, an innovative IOFB for multiple contaminants detection in water samples with high sensitivity and excellent selectivity was developed. To the best of our knowledge, this report is the first on a sensitive, rapid and cost-effective assay and early warning system based on TriPleX™ technology waveguide on a FS substrate for environmental contaminants risk in water sample. This system has a number of distinct advantages over traditional detection technologies. First, the CMOS compatible TriPleX™ technology shows low mass production costs, while at the same time its low loss, on-chip spotsize convertors allows for low loss fiber-chip coupling while maintaining high chip surface intensity and low patch-to-patch deviation. Second, this system demonstrates sufficient sensitivity with the LOD of 0.22 μg/L, 1.18 μg/L, 0.2 μg/L and 0.06 μg/L towards MC-LR, 2,4-D, atrazine and BPA even in the presence of interfering substances in environmental matrices. Finally, the IOFB exhibits robustness and ruggedness in long-term monitoring, allows for simultaneous detection from the bottom side and

fluid manipulation on the top side through the use of FS as substrate material, while the biochip is reproducible and verifiable. More importantly, our biochip contains thirty-two sensing points, which allows the simultaneous determination of thirty-two different pollutants when the sensing windows are modified with different analyte conjugates with matching fluorescence-labeled antibodies used. Thus, the IOFB reported herein is a flexible and powerful platform for the bioassay of environmental multi-contaminants to satisfy the high demand of ensuring the safety of water environment.

## Acknowledgement

This research is supported by the Major Scientific Equipment Development Project of China (2012YQ030111).

## Appendix A. Supporting information

Supplementary data associated with this article can be found in the online version at http://dx.doi.org/10.1016/j.bios.2018.01.066.

## References

Anderson, G.P., Breslin, K.A., Ligler, F.S., 1996. ASAIO J. 42 (6), 942–946.
Axelrod, D., Burghardt, T.P., Thompson, N.L., 1984. Ann. Rev. Biophys. Bioeng. 13 (1), 247–268.
Besselink, G., Heideman, R., Schreuder, E., Wevers, L., Falke, F., Van den Vlekkert, H., 2016. J. Biosens. Bioelectron. 7 (2), 209.
Chalyan, T., Guider, R., Pasquardini, L., Zanetti, M., Falke, F., Schreuder, E., Heideman, R.G., Pederzolli, C., Pavesi, L., 2016. Biosensors 6 (1), 1–10.
Colomer-Farrarons, J., Miribel-Català, P.L., Rodríguez-Villarreal, A.I., Samitier, J., 2011. InTech., Rijeka, pp. 373–400.
Damen, C., Heideman, R.G., Heesink, G.J., Schreuder, E., 2014. Latin America Optics and Photonics Conference Optical Society of America, LF2D-1.
De Vos, K., Bartolozzi, I., Schacht, E., Bienstman, P., Baets, R., 2007. Opt. Express 15 (12), 7610–7615.
Densmore, A., Xu, D.-X., Waldron, P., Janz, S., Cheben, P., Lapointe, J., Delge, A., Lamontagne, B., Schmid, J., Post, E., 2006. IEEE Photon. Technol. Lett. 18 (23), 2520–2522.
Duer, R., Lund, R., Tanaka, R., Christensen, D.A., Herron, J.N., 2010. Anal. Chem. 82 (21), 8856–8865.
Fédéli, J.M., Vivien, L., Smit, M.K., 2013. In: Proceedings of the SPIE. 8767, 876701-876710.
Han, S.T., Zhou, X.H., Tang, Y.F., He, M., Zhang, X., Shi, H.C., Xiang, Y., 2016. Biosens. Bioelectron. 80, 265–272.
Heideman, R.G., Hoekman, M., Schreuder, E., 2012. IEEE J. Sel. Top. Quantum 18 (5), 1583–1596.
Heideman, R.G., Geuzebroek, D.H., Leinse, A., Melloni, A., Morichetti, F., Roeloffzen, C.G. H., Driessen, A., 2007. In: Proceedings of the European Conference on Integrated Optics.
Hirschfeld, T., 1965. Can. Spectrosc. 10 (5), 128.
Homola, J., 2003. Anal. Bioanal. Chem. 377 (3), 528–539.
Hua, P., Hole, J.P., Wilkinson, J.S., Proll, G., Tschmelak, J., Gauglitz, G., Kaiser, J., 2005. Opt. Express 13 (4), 1124–1130.
Huang, S.H., Tseng, F.G., 2005. J. Micromech. Microeng. 15 (12), 2235–2242.
Lambeck, P.V., 1992. Sens. Actuators B Chem. 8 (1), 103–116.
Lambeck, P.V., 2006. Meas. Sci. Technol. 17 (8), R93–R116.
Leinse, A., Heideman, R., Beeker, W., et al., 2012. In: Proceedings of the 16th European Conference on Integrated Optics, ECIO 2012.
Ligler, F.S., Conrad, D.W., Golden, J.P., Feldstein, M.J., MacCraith, B.D., Balderson, S.D., Rowe-Taitt, C.A., 1998. Int. Soc. Opt. Photonics 3258, 50–56.
Lin, Y., Li, D., Zeng, S., He, M., 2016. Front. Environ. Sci. Eng. 10 (3), 539–547.
Liu, L.H., Zhou, X.H., Xu, W.Q., Song, B.D., Shi, H.C., 2014. RSC Adv. 4 (104), 60227–60233.
Liu, L.H., Zhou, X.H., Lu, M.F., Zhang, M.K., Yang, C., Ma, R.M., Memon, A.G., Shi, H.C., Qian, Y., 2017a. Sens. Actuators B Chem. 240, 107–113.
Liu, L.H., Zhou, X.H., Lu, Y., Shan, D.D., Xu, B., He, M., Shi, H.C., Qian, Y., 2017b. Biosens. Bioelectron. 97, 16–20.
Liu, L.H., Zhou, X.H., Wilkinson, J.S., Hua, P., Song, B.D., Shi, H.C., 2017c. Sci. Rep. 7 (1), 3655.
Long, F., He, M., Shi, H.C., Zhu, A.N., 2008. Biosens. Bioelectron. 23 (7), 952–958.
Long, F., He, M., Zhu, A.N., Shi, H.C., 2009. Biosens. Bioelectron. 24 (8), 2346–2351.
Long, F., Zhu, A., Zhou, X., Wang, H., Zhao, Z., Liu, L., Shi, H., 2014. Biosens. Bioelectron. 55, 19–25.
Mauriz, E., Calle, A., Lechuga, L.M., Quintana, J., Montoya, A., Manclus, J.J., 2006. Anal. Chem. Acta 561 (1), 40–47.
Misiakos, K., Raptis, I., Salapatas, A., Makarona, E., Botsialas, A., Hoekman, M., Stoffer, R., Jobst, G., 2014. Opt. Express 22 (8), 8856–8870.
Prak, A., Leeuwis, H., Heideman, R., Leinse, A., Borst, G., 2011. Proc. SPIE 7928, 79280L–79281L.
Robbins, D.J., Lechuga, L.M., Jabbour, G.E., Sepulveda, B., Sanchez del Rio, J., Blanco, F., Calle, A., Dominguez, C., 2004. Proc. SPIE 5357, 96–110.
Shi, H.C., Song, B.D., Long, F., Zhou, X.H., He, M., Lv, Q., Yang, H.Y., 2013. Environ. Sci. Technol. 47 (9), 4434–4441.
Singh, S., Srivastava, A., Oh, H.M., Ahn, C.Y., Choi, G.G., Asthana, R.K., 2012. Toxicon 60 (5), 878–894.
Wörhoff, K., Heideman, R.G., Leinse, A., Hoekman, M., 2015. Adv. Opt. Technol. 4 (2), 189–207.
Wiki, M., Gao, H., Juvet, M., Kunz, R.E., 2001. Biosens. Bioelectron. 16 (1), 37–45.
Xu, D.X., Densmore, A., Delâge, A., Waldron, P., McKinnon, R., Janz, S., Lapointe, J., Lopinski, G., Mischki, T., Post, E., 2008. Opt. Express 16 (19), 15137–15148.
Zhou, X.H., Liu, L.H., Xu, W.Q., Song, B.D., Sheng, J.W., He, M., Shi, H.C., 2014a. Sci. Rep. 4, 4572.
Zhou, X.H., Song, B.D., Shi, H.C., Liu, L.H., Guo, H.L., He, M., 2014b. Sens. Actuators B Chem. 198, 150–156.
Zhu, L., Zhou, X.H., Shi, H.C., 2013. Front. Environ. Sci. Eng. 8 (6), 945–951.